ACS APPLIED MATERIALS & INTERFACES

Research Article

www.acsami.org

Sputter-Deposition of Silver Nanoparticles into Ionic Liquid as a Sacrificial Reservoir in Antimicrobial Organosilicate Nanocomposite Coatings

Steven C. Hamm,[†] Ravi Shankaran,[†] Venu Korampally,*[,†] Sangho Bok,[†] Snigdha Praharaj,[†] Gary A. Baker,*[,‡] J. David Robertson,[‡,§] Byung Doo Lee,[⊥] Shramik Sengupta,[⊥] Keshab Gangopadhyay,[#] and Shubhra Gangopadhyay*[,†,⊥]

[†]Department of Electrical and Computer Engineering, University of Missouri, Engineering Building West, Columbia, Missouri 65211, United States

[‡]Department of Chemistry, University of Missouri, 601 S. College Avenue, Columbia, Missouri 65211, United States

[§]University of Missouri Research Reactor Center, University of Missouri, 1513 Research Park Drive, Columbia, Missouri 65211, United States

[⊥]Department of Biological Engineering, University of Missouri, 1406 E. Rollins Street, Columbia, Missouri 65211, United States

[#]Nanos Technologies LLC, 2306 Longview Drive, Columbia, Missouri 65203, United States

Supporting Information

ABSTRACT: We present a new approach for fabricating robust, regenerable antimicrobial coatings containing an ionic liquid (IL) phase incorporating silver nanoparticles (AgNPs) as a reservoir for Ag^0/Ag^+ species within sol–gel-derived nanocomposite films integrating organosilicate nanoparticles. The IL serves as an ultralow volatility (vacuum-compatible) liquid target, allowing for the direct deposition and dispersion of a high-density AgNP "ionosol" following conventional sputtering techniques. Two like-anion ILs were investigated in this work: methyltrioctylammonium bis(trifluoromethylsulfonyl)imide, $[N_{8881}][Tf_2N]$, and 1-ethyl-3-methylimidazolium bis(trifluoromethylsulfonyl)imide, $[emim][Tf_2N]$. Silver ionosols derived from these two ILs were incorporated into silica-based sol–gel films and the resultant antimicrobial activity evaluated against *Pseudomonas aeruginosa* bacteria. Imaging of the surface morphologies of the as-prepared films established a link between an open macroporous film architecture and the observation of high activity. Nanocomposites based on $[N_{8881}][Tf_2N]$ displayed excellent antimicrobial activity against *P. aeruginosa* over multiple cycles, reducing cell viability by 6 log units within 4 h of contact. Surprisingly, similar films prepared from $[emim][Tf_2N]$ presented negligible antimicrobial activity, an observation we attribute to the differing abilities of these IL cations to infiltrate the cell wall, regulating the influx of silver ions to the bacterium's interior.

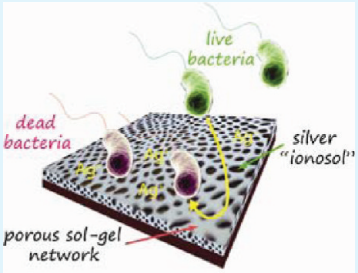

KEYWORDS: *antibacterial, sol–gel, polymethsilsesquioxane, ionic liquid, silver nanoparticles, Pseudomonas aeruginosa*

INTRODUCTION

Silver (Ag) has been a widely used antimicrobial agent in various materials, processes, and applications since ancient times.[1] Materials incorporating Ag in the form of nanoparticles, ions, alloys, or compounds have long been known to exhibit antimicrobial properties. These various forms of Ag ionize when in contact with water to form Ag^+, which has a strong interaction to biological molecules containing thiols, including enzymes and bacterial cell membranes. This strong interaction denatures enzymes and causes cellular damage, ultimately leading to cell death. The Ag^+ ion further bonds to bacterial cell DNA, preventing the cell from replicating.[1,2] It has been found that not only is Ag effective against a broad range of microorganisms in the body (over 650 disease-causing organisms), but it remarkably has no negative side-effects on the human body when present at sufficiently low levels.[3] This feature of Ag/Ag^+ has been utilized for a large number of applications in the environmental, food, clinical/medical, and other fields.[2,4−6]

The activity and stability of Ag is believed to be influenced by the nature of the supporting matrix used for its immobilization/entrapment.[7,8] An ideal matrix is one that remains antimicrobial after mechanical wear, enables good uniformity of Ag throughout the coating, and allows constant interaction between Ag species and bacteria without leaching upon repeated use. A common method employed to endow materials with antimicrobial properties is to modify surfaces with chemically bound antimicrobial compounds or silver.[9−13] Surface chemical modification requires compounds with unique functionalized groups to attach the silver, limiting the application of each compound to specific kinds of substrates. Additionally, these methods are not mechanically robust and the functionalized layer can generally be removed by abrasion or delamination over time. Despite the

Received: September 9, 2011
Accepted: December 26, 2011
Published: January 11, 2012

interesting characteristics demonstrated with these coatings, further improvement in terms of robustness, stability, distribution, and compatibility of the Ag within the supporting matrix is desired to enhance performance in real-world settings.

Sol−gel-based silicate materials are advantageous in this regard as they have good control on site selective immobilization and uniform distribution of Ag within the silicate matrices with good stability. Sol−gel inorganic systems are additionally highly inert and biocompatible, coupled with extreme thermal stability, thereby offering enhanced physicochemical properties relative to their polymeric counterparts.[14−17]

Sol−gel chemistry generally involves the synthesis of materials by hydrolysis and (poly)condensation of suitable molecular precursors, which offers a simple and inexpensive means for fabricating inorganic coatings, fibers, monolithic structures and other arbitrary geometries.[14,16−18] However, preparing flexible and robust coatings using this technique remains a significant challenge. Drying-induced shrinkage (syneresis) and subsequent cracking is a common problem with sol−gel-based processing. In addition, these processes are highly susceptible to moisture and the materials fabricated are typically brittle unless polymeric additives or plasticizers are added, which may significantly interfere with the material's intended functionality. In our laboratory, we have synthesized 3-nm sized poly(methylsilsesquioxane) (PMSSQ) OSNPs that can be used in combination with sol−gel processes to achieve nanocomposite coating materials with unprecedented tunability in their physical and chemical characteristics.[19] In these reports, we have demonstrated the advantages of the PMSSQ_NP sol−gel composite as a novel host matrix for the immobilization of suitable additives for various applications. Among the materials that can be incorporated within the sol−gel layer nanocomposite are metallic nanoparticles (like AgNPs) and ionic liquids (ILs). ILs are low-temperature molten salts; that is, they are liquids composed entirely of ions. These salts are characterized by fairly weak interionic interactions, because of the pairing of a large, asymmetric cation and a charge-delocalized anion. ILs have a number of interesting characteristics such as negligible vapor pressure, high polarity, intrinsic ionic conductivity, and excellent chemical and thermal stability.

The aim of the current study was to explore the possibility of obtaining high-performance antimicrobial coatings based upon incorporating into a sol−gel nanocomposite film an IL phase containing AgNPs deposited via magnetron sputtering. Direct nanoparticle formation within ILs by sputter deposition presents an intriguing and potentially cleaner (e.g., ligand-free) avenue compared with conventional wet-chemistry approaches, including those based on hydrogen-assisted reduction for in situ particle formation, in that no external structure-directing agents are required nor byproducts created. In particular, byproducts generated from conventional methods require additional steps for their removal in order that they do not negatively interfere with or complicate the desired functionality of the nanoparticle, whether antimicrobial,[20] catalytic,[21] biosensory,[22] and so forth. In this work, a high concentration density of silver nanoparticles was directly sputtered into an IL phase and the resulting "silvered" IL was then introduced into a conventional sol−gel formulation containing PMSSQ nanoparticles. During sputtering, the IL served as an efficient matrix for controlling and stabilizing Ag cluster growth, enabling the uniform distribution of Ag throughout the fluid, a characteristic thought to be highly desirable for ensuring sufficient contact and interaction between Ag and microbial species at the surface of antimicrobial coatings. Indeed, for one selected IL, the resulting Ag-dispersed nanocomposite film showed excellent antimicrobial activity against a representative microorganism, *P. aeruginosa*, a ubiquitous bacterium that is clinically important in a range of health problems such as dermatitis and countless infections affecting the urinary tract, lungs, kidneys, respiratory system, soft tissues, bones, joints, and the gastrointestinal tract. Because *P. aeruginosa* thrives on most surfaces, this bacterium is also problematic for medical equipment, particularly catheters, causing cross-infections in hospitals and clinical settings. The present study reveals that PMSSQ_NP sol−gel composites containing a particular silvered IL phase exhibit excellent sustained activity against *P. aeruginosa*. We also find that the choice of IL is of the utmost importance, as yet another IL phase yields materials with essentially no activity against this bacterium despite their containing a similar level of Ag. Furthermore, as the sol−gel process proceeds, the initially well-formed AgNPs deposited by sputtering become smaller and are mostly etched away and oxidized, giving rise to a reservoir of antimicrobial Ag^+ species responsible for the activity.

MATERIALS AND METHODS

Preparation of "Silvered" Ionic Liquid. Sol−gel organosilicate nanocomposite coatings were prepared with and without incorporating IL. Two different ILs were included in this study: methyltrioctylammonium bis(trifluoromethylsulfonyl)imide ($[N_{8881}][Tf_2N]$) and 1-ethyl-3-methylimidazolium bis(trifluoromethylsulfonyl)imide ($[emim][Tf_2N]$). The $[emim][Tf_2N]$ was purchased from Covalent Associates, Inc. (Corvallis, OR) and $[N_{8881}][Tf_2N]$ was synthesized in-house following procedures described in detail elsewhere.[23]

Coatings were prepared by incorporating 9.3 and 14.6 wt % IL relative to the weight of the final coating. Additionally, the incorporation of each fraction of IL into the coating was carried out for both pure IL and IL containing a high concentration of AgNPs (~0.33 wt %) generated by magnetron sputtering deposition of AgNPs directly into the IL. This technique, which requires the use of high vacuum, can be used in the present situation due to the essentially null vapor pressures of common ILs.[24−27] Approximately 1−1.5 mL of the IL was spread over a clean silicon substrate to form a thin film followed by introduction into the sputtering system (ATC 2000 V, AJA International Inc., N. Scituate, MA). Silver was deposited using a 3 inch target (99.99%, Kurt J. Lesker) at 30 W for 30 min using an Ar flow rate of 20 sccm, chamber pressure of 4 mTorr, and a target-to-substrate distance of 6 inches. The resulting AgNP−containing ILs were transferred to 2 mL glass vials by carefully scraping the film off the substrate. Transmission electron microscopy (TEM) was used to characterize the size and morphology of the AgNPs generated within the ILs.

Preparation of Silica Sol−Gels. Tetraethylorthosilicate (TEOS, 98%), methyltrimethoxysilane (MTMS, 98%), ethanol (200 proof), and hydrochloric acid (37% ACS) were purchased from Sigma-Aldrich (St. Louis, MO). Polymeric silica sol was prepared by a two-step process as detailed in ref 28 using MTMS in addition to TEOS as silica source. Briefly, a stock solution of silica sol was prepared from an equimolar mixture of TEOS and MTMS using HCl as catalyst. Initially, TEOS and MTMS were partially hydrolyzed by mixing TEOS, MTMS, ethanol, water, and HCl in the molar ratio $0.5:0.5:3:1:5 \times 10^{-5}$ and refluxing at 60 °C for 75 min. Following this prehydrolysis step, additional water (5 mol equiv) and HCl (0.13 equiv) were added into the solution. The solution was stirred at 25 °C for 15 min on a hot plate then aged in a 50 °C bath for another 15 min. Finally, ethanol (22 equiv) was added and the mixture was aged at ambient temperature for two days before use. The final reactant molar ratios of TEOS, MTMS, ethanol, water, and HCl in the sol were essentially 0.5:0.5:25:6:0.13.

PMMSQ Nanoparticle Preparation. Polypropylene glycol (PPG, average molecular weight 425) was purchased from Sigma-Aldrich (St. Louis, MO) and PMSSQ flakes (GR650F) were purchased from Techneglas Inc. (Perrysburg, OH) for the preparation of PMSSQ_NPs. The nanoparticles were prepared through polymer collapse, following methods described previously.[29] First, a 50 wt % solution of PMSSQ was prepared by dissolving 50 g of PMSSQ in 50 g of ethanol. A 50 wt % solution of PPG was also prepared in ethanol. The PMSSQ and PPG solutions were mixed together in a 1:1 (w/w) ratio, thoroughly vortexed, and ultrasonicated for 2 to 3 min. The mixture was poured into a 400 mL open beaker and heated at 75 °C under continuous

dx.doi.org/10.1021/am2012273 | ACS Appl. Mater. Interfaces 2012, 4, 178−184

stirring to form the PMSSQ nanoparticles through enrichment of the relative concentration of PPG within the solution by evaporation of ethanol. The heating process was continued until ~34 g of ethanol was evaporated following which the solution was allowed to cool down to room temperature naturally. 100 g of the resulting solution was combined with 400 mL of ethanol in a 500 mL beaker. Next, 15 mL of chlorotrimethylsilane (TMCS) was added, 5 mL at a time, followed by mixing using a magnetic stirring bar for 2 min. The addition of TMCS resulted in a cloudy solution due to the rapid precipitation of PMSSQ NPs. TMCS effectively reacts with the surface hydroxyl groups on the PMSSQ NPs thereby imparting sufficient hydrophobicity to induce precipitation in the relatively polar ethanol. The solution was kept overnight at room temperature to allow the particles to fully precipitate from solution. The resulting supernatant was carefully decanted and the precipitated solid mass was dried under flowing nitrogen. The particles were then redispersed in propylene glycol monomethyl ether acetate (PMA) to yield a clear solution containing a particle concentration of 230 mg/mL.

Preparation of OSNP Silica Sol–Gel Films. The above PMSSQ NP stock solution (230 mg/mL in PMA) was combined with MTMS-TEOS sol in ethanol at a ratio of 3:2 (v/v). This ratio was found to give the best quality, most durable coatings that displayed good surface hydrophobicity and wear resistance (results not presented here). Ionic liquids with and without AgNPs were added to this formulation to a final relative concentration of 9.3 wt % and 14.6 wt % to study the effect of different concentrations in the film. The solution was ultrasonicated for 2–3 min to achieve a homogeneous, clear solution, and let stand for at least 1 h before proceeding. 1.25 mL of the above formulation was heated under stirring on a hot plate set to 80 °C and 50 μL of 3-aminopropyltriethoxysilane (APTES) was subsequently added. APTES enhances the cross-linking of the sol–gel matrix with the PMSSQ NPs thereby reducing phase separation of the nanoparticles upon curing and resulting in a well cross-linked coating at low curing temperatures. After the APTES addition, the solution continued to be heated under stirring for an additional 1 min before drop-casting on regular microscope glass slides (Fisher Scientific). The films were cured at 95 °C for ~12 h in a gravity convection oven and stored at room temperature before subjecting them to antimicrobial activity testing.

Ag Concentration Analysis. AgNP-doped $[N_{8881}][Tf_2N]$ was incorporated into PMSSQ NP sol–gel films and undoped $[N_{8881}][Tf_2N]$ to various amounts (0–21.8 wt %) to estimate the Ag concentration in the studied films. The concentration of Ag was determined by standard comparator instrumental neutron activation analysis. The samples were weighed into 1/4-dram high-density polyethylene vials. The samples were then capped and irradiated for 7 s in a thermal neutron flux of approximately 6.5×10^{13} n cm^{-2} s^{-1}. The samples were real-time counted for 60 s at a sample-to-detector distance of approximately 3 cm following a 120 s decay. The spectrometer consisted of a 25% high-purity germanium detector with a full-width-half-maximum resolution of 1.9 keV at 1331 keV. The mass of Ag was quantified using the 657.8 keV peak from the decay of ^{110}Ag which has a half-life of 24.6 s. The comparator standards were prepared gravimetrically from a certified Ag standard solution (High Purity Standards). The average response factor from the analysis of three 15 μg Ag standards used in the comparator analysis was 589.4 ± 1.0 counts/μg.

Preparation of Bacterial Samples. *P. aeruginosa* cultures were originally purchased from Wards Natural Science, USA and subcultured in the lab by growing on tryptic soy broth (TSB)/agar (both purchased in powder form from Bioworld, USA and prepared as per instructions). Fresh colonies of the *P. aeruginosa* bacteria were obtained by streak-plating a small amount of the stock solution on tryptic soy agar (TSA) plates and incubating them at 37 °C for 48 h. At the beginning of each experiment, a single bacterial colony was picked up using an inoculation loop and dispersed into 10 mL of TSB. The broth was loaded into an incubator-shaker for 48 h at 37 °C. The resulting solution contains ~1×10^8 bacterial colony forming units (CFU)/mL. One milliliter of the same was transferred into a centrifuge tube and centrifuged for 3 min at a speed of 5000 rpm. The supernatant media was removed and the bacteria settled at the bottom of the tube were resuspended in 1 mL of sterile phosphate buffered saline (PBS) solution and vortexed. This solution, also containing ~1×10^8 CFU/mL of bacteria, was serially diluted by 2 orders of magnitude to obtain suspensions with ~1×10^6 CFU/mL of *P. aeruginosa* in PBS solution.

Antimicrobial Studies. The antimicrobial activity of the PMSSQ NP sol–gel films (with and without AgNPs), with different ILs included, was evaluated using *P. aeruginosa* bacteria. A Hybriwell (a stick-on silicon rubber gasket, 150 μm thick, with a transparent, but impermeable top) was attached to the surface of interest, and a 15 mL suspension of bacteria (~1×10^6 CFU/mL of *P. aeruginosa* in PBS) was loaded into the region enclosed by the Hybriwell. The system was then allowed to incubate at 37 °C for a selected duration of time. At the desired duration, the suspension was harvested, and the number of bacteria that remain viable were evaluated by serial ten-fold dilution and plating.

A wider variety of surfaces were initially evaluated for antimicrobial activity by incubating the samples as described above for 24 h. A second experiment was conducted for samples that demonstrate an ability to reduce bacterial numbers significantly more than the control (Hybriwell on plain glass slide). Here multiple samples of each coating type were brought in contact with *P. aeruginosa* in a Hybriwell as previously, but one sample is harvested after each short interval of time (typically, 2 h) and the number of viable bacteria evaluated. This allowed a more fine-grained estimate of the relative antimicrobial efficacy of the substrates.

Both types of ILs were investigated in the initial experiment. As discussed in detail in the next section, $[emim][Tf_2N]$ with Ag was found not to show any antimicrobial properties, so only $[N_{8881}][Tf_2N]$ was examined in the second set of experiments. In the second round of experiments, the coatings examined and the corresponding Ag concentrations are listed in Table 1. As shown, they consist of (1) a plain glass slide, (2) PMSSQ NP sol–gel film (containing no ILs and no AgNPs), (3) PMSSQ NP sol–gel film with 9.3 wt % IL included within (but no AgNPs), (4) PMSSQ NP sol–gel film with 9.3 wt % AgNP-doped IL, (5) PMSSQ NP-sol–gel film coating with 14.6 wt % IL, and (6) PMSSQ NP-sol–gel coating with 14.6 wt % AgNP-doped IL.

Table 1. Summary of Composite Films Tested for Antimicrobial Activity using $[N_{8881}][Tf_2N]$

sample	wt% IL	Ag concentration (ppm)
(1) glass slide	0	0
(2) PMSSQ NP sol–gel	0	0
(3) PMSSQ NP sol–gel	9.3	0
(4) PMSSQ NP sol–gel	9.3	12.7
(5) PMSSQ NP sol–gel	14.6	0
(6) PMSSQ NP sol–gel	14.6	19.1

RESULTS AND DISCUSSION

Figure 1a shows the TEM image of the obtained PMSSQ NPs. The particle sizes ranged from 3 to 7 nm with a mean particle size of 3.5 nm. As the synthesis technique does not involve the use of high temperature processing conditions, the as-formed nanoparticles are not fully cross-linked and hence may be classified as 'soft' nanoparticles. Figure 1b shows the FTIR plot of the obtained nanoparticles after the TMCS treatment. It is noteworthy that although TMCS effectively reacts with the surface hydroxyl groups present on the nanoparticles which leads to their eventual precipitation from ethanolic solution, there still remains enough unreacted –OH functionality on the surface of the nanoparticles that may be used to further functionalize the nanoparticles or graft them to various matrices. This is evident both from the FTIR plots (peaks in the region 930 cm^{-1} corresponding to Si–OH stretching vibration[30] from surface groups) and from the fact that films could still be spin coated from this nanoparticulate dispersion to obtain smooth, continuous films. On the contrary, particles that have been reacted twice with TMCS (by redispersing them in ethanol followed by a second TMCS treatment) lose the ability to form continuous films due to the

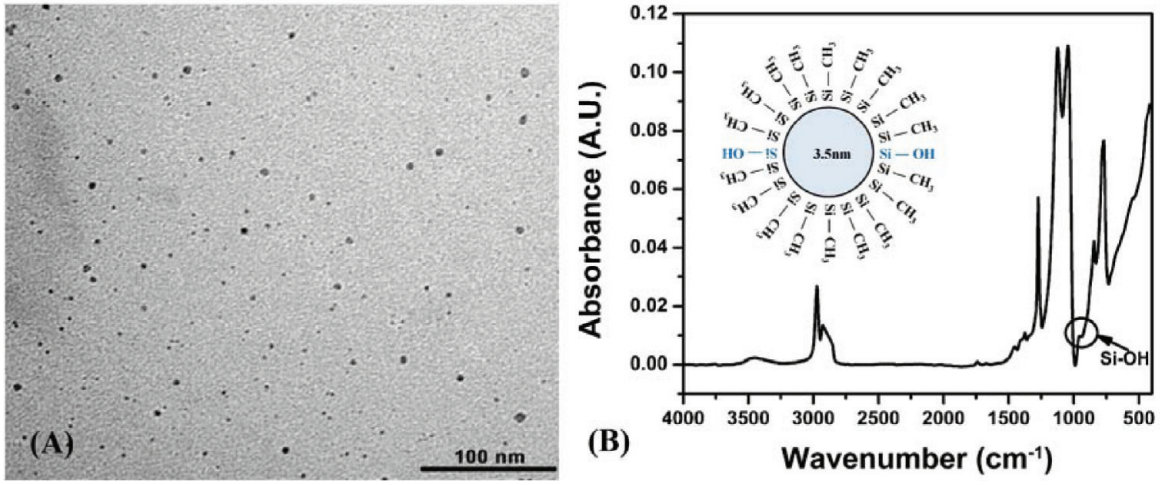

Figure 1. (A) TEM image of PMSSQ NPs. (B) FTIR plot of the obtained nanoparticles after the TMCS treatment (inset: schematic of a TMCS-treated nanoparticle showing its surface functionality).

silanization of all surface silanols. A description of the other peaks observed in the FTIR plot may be found in ref 18.

The $[N_{8881}][Tf_2N]$ was prepared as a transparent liquid which turned a dark yellow after AgNP incorporation as seen in Figure 2.

Figure 2. $[N_{8881}][Tf_2N]$ before (left) and after (right) Ag deposition.

UV−visible absorption spectrum of the AgNP-doped IL, shown in Figure 3, was measured by diluting the IL 1:1 by weight with ethanol within a 1 mm thick quartz cuvette. The IL was diluted because the concentration of Ag was too high, causing the measurement to saturate. The plot reveals an absorption peak around 410 nm, which is consistent with the absorption peak of AgNPs due to their surface plasmon resonance (SPR).[31] TEM analysis was performed on the AgNP-doped IL by soaking 5 μL of the IL on a carbon grid for 5 min which was subsequently dipped into ethanol to dissolve the IL prior to imaging. The TEM image in Figure 4 shows nanoparticles are 5−10 nm in diameter with an average size of 7.5 nm.

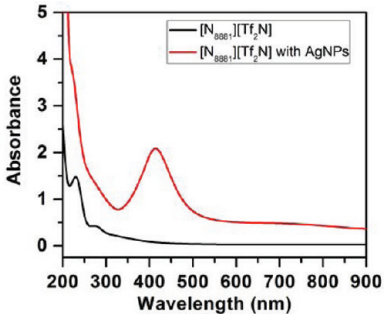

Figure 3. UV−vis absorption spectra of $[N_{8881}][Tf_2N]$ with and without AgNPs measured against an air background (path length: 1 mm). Samples were diluted 1:1 (w/w) with ethanol for ease of handling.

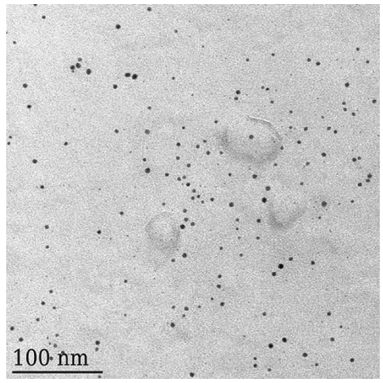

Figure 4. TEM image of AgNPs deposited into $[N_{8881}][Tf_2N]$.

UV−vis absorbance spectral profiles of the nanocomposite films suggested that Ag was no longer present in colloidal form or the particle sizes had become too small to support a SPR band, suggesting that the AgNPs initially present were etched away and very likely oxidized. Evidence in support of this notion was found by adding an equivalent amount of HCl to AgNPs in IL diluted in ethanol, which clearly resulted in loss of the AgNP SPR peak (see Figure S1 in the Supporting Information). It is suggested from this experiment that the AgNPs reacted with HCl to form AgCl due to the high reactivity of the two components.[32] This result was verified by X-ray diffraction (XRD) using a Rigaku Ultima IV XRD and a Cu K_α source. Figure S2 in the Supporting Information shows the diffraction peaks for fcc Ag resulting from AgNPs present within $[N_{8881}][Tf_2N]$. These peaks are no longer present for sample 6. The in situ formation of AgCl within the nanocomposite films from AgNPs initially present within

dx.doi.org/10.1021/am2012273 | ACS Appl. Mater. Interfaces 2012, 4, 178−184

$[N_{8881}][Tf_2N]$ was not our intention, however, other Ag species such as AgCl indeed exhibit strong antimicrobial characteristics due to the dissociation of Ag^+ ions.[33] As the original motivation for this study was the exploration of Ag sputter-deposited IL as a vehicle for transferring Ag-based antimicrobial activity to our organosilicate nanocomposite films, the precise nature of the Ag within the film is not cause for alarm in the current work. It is evident, however, that future antimicrobial materials and surfaces might be possible by direct exploitation of ILs which contain complexed Ag^+ as an integral portion of the cationic species.[34]

In Figure 5, we show AFM images of samples 2, 5, and 6 which are representative of −/−, +/−, and +/+ samples in terms

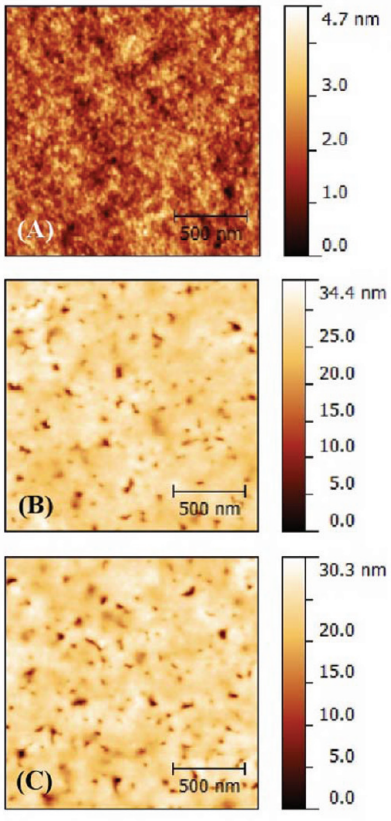

Figure 5. AFM images of (A) sample 2, (B) sample 5, and (C) sample 6.

of whether they contain $[N_{8881}][Tf_2N]$/Ag, respectively. As can be seen, the coatings containing IL consist of a highly porous network with macropores in the 100−200 nm range, whether or not Ag is present. This open porous morphology is not seen for coatings that lack IL. A FEI Quanta 600F scanning electron microscope (SEM) was used to image the cross-section of sample 6 (Figure 6). This image reveals that the coating is evenly porous throughout the film. It was also observed that even in the presence of these large structures, which one would expect to cause considerable light scattering, the films were remarkably transparent. This observation led us to conclude that the pits/pores comprised IL nanopools that uniformly phase segregated within the coating into discrete domains. Apparently, the close index matching between the ILs ($n \approx 1.45$) and the sol−gel nanocomposite ($n \approx 1.42$) matrix essentially helped to mitigate light scattering. Further, subjecting the films to temperatures above the decomposition temperature for $[N_{8881}][Tf_2N]$ (>300 °C) resulted in films that scattered light strongly, although AFM images of

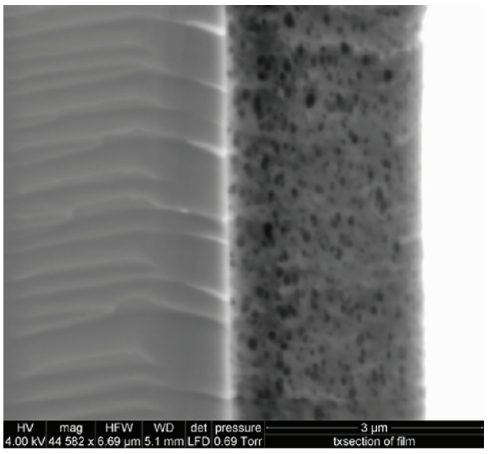

Figure 6. Cross-sectional SEM image of sample 6.

their surfaces were found to remain fairly similar in morphology before and after such calcination.

Neutron activation analysis was chosen as the method of determining Ag concentrations because this method has a much higher precision (~1 ppm) than energy dispersive spectroscopy (EDS) or X-ray photoelectron spectroscopy (XPS). The Ag concentration was low enough within these films that EDS and XPS were unable to detect any trace of Ag (see Table S1 in the Supporting Information). Therefore, Ag concentrations within samples 4 and 6 were estimated from neutron activation analysis of different concentrations of AgNP-doped $[N_{8881}][Tf_2N]$ within PMSSQ NP sol−gel and undoped $[N_{8881}][Tf_2N]$ (see Figure 7).

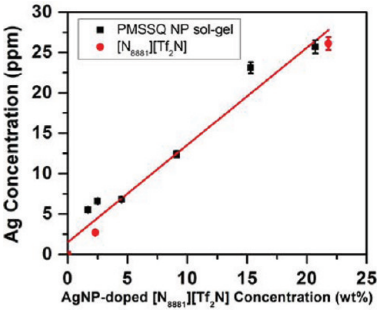

Figure 7. Neutron activation analysis of various AgNP-doped $[N_{8881}][Tf_2N]$ concentrations within PMSSQ NP sol−gel films and undoped $[N_{8881}][Tf_2N]$.

Using the linear fit of the measured data, we estimate the amount of Ag within samples 4 and 6 to be approximately 12.7 ppm and 19.1 ppm by weight, respectively.

The first set of tests was conducted to gauge the effect of the choice of IL on the overall antimicrobial efficacy of the nanocomposite. As Figure 8 shows, irrespective of the presence of AgNPs, inclusion of the IL $[emim][Tf_2N]$ results in no discernible antimicrobial function for the coating. In surprising contrast, use of $[N_{8881}][Tf_2N]$ containing AgNPs clearly generates an antimicrobial material. We attribute this striking difference to a dual-mode action of Ag ions in concert with the quaternary ammonium ion of $[N_{8881}][Tf_2N]$. Certainly, onium ions have long been used as biocides, typically with alkyl chain lengths around 14 or higher, although shorter chain lengths have also shown signs of antimicrobial characteristics.[8,35,36] It is theorized that the octyl chains of the $[N_{8881}]^+$ cation in $[N_{8881}][Tf_2N]$ are first adsorbed onto the cell surface by electrostatic and hydrophobic interactions. Diffusion through the cell

dx.doi.org/10.1021/am2012273 | ACS Appl. Mater. Interfaces 2012, 4, 178−184

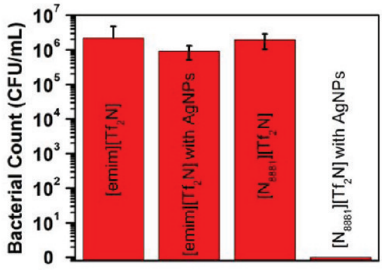

Figure 8. Antimicrobial activity of sol−gel nanocomposite films with two different ILs. (9.3 wt %, incubation time: 24 h).

wall damages the cytoplasmic membrane of the bacteria, thereby allowing the Ag ions to penetrate the compromised cell wall and inactivate proteins (e.g., by reaction with thiol groups of Cys, disulfide linkages), disrupting the DNA machinery and causing cell death.[1,2] However, based upon our findings, owing to its short alkyl chain, $[emim][Tf_2N]$ may sorb to the cellular surface but appears unable to heavily damage the cell wall, such that Ag^+ ions cannot penetrate the cell to arrest cellular function. On the basis of this scenario, further experiments were confined to the use of $[N_{8881}][Tf_2N]$ in our nanocomposites.

The antimicrobial activities of the samples listed in Table 1 were studied further by performing assays with an incubation period from 2 to 8 h at 2 h intervals. The bacterial colonies were counted using iterative ten-fold (decadic) dilutions which were made and plated separately for each sample collected.

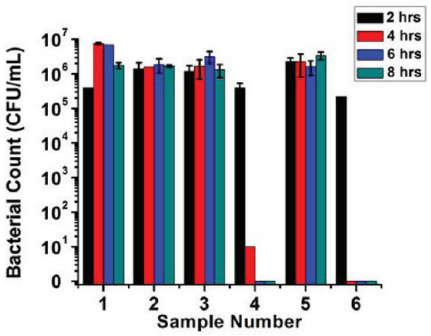

Figure 9. Bar graph showing the antimicrobial activity of the Ag films and control films against *P. aeruginosa* bacteria tested for 2 to 8 h of incubation with 2 h intervals. The deviations of the bacterial counts were taken from decadic serial dilutions.

Figure 9 illustrates the results of these antibacterial tests alongside controls 1−3 and 5, for *P. aeruginosa* (a Gram-negative, aerobic opportunistic pathogen) on agar plates for the incubation times studied. As can be seen, films initially containing AgNPs showed significant inhibition of the growth of the bacteria, essentially killing all bacterial colonies within 4 h, whereas well grown bacterial colonies were observed with Ag-free controls. These results clearly indicate that the Ag-incorporated nanocomposite films possess highly potent antibacterial properties against *P. aeruginosa*. We observed 6 log inhibition of the bacterial growth, indicating excellent antibacterial promise for these materials.

It is reasonable to suggest that the binding of the onium ion and Ag^+ to the bacterial surface must depend on the nanocomposite surface area available for such interactions. That is, a desirable film configuration should promote onium ion and Ag^+ contact with the external environment (i.e., bacteria). Certainly, the high antimicrobial activity exhibited by these films is due, at least in part, to the large surface area generated by the highly porous morphology observed for these films. Moreover, the unique morphology of the nanocomposite permits a uniform distribution of the $[N_{8881}]^+$ and Ag^+ cations within the film, as well as their presentation at the film's external surface. It is thus likely that the unique structural features associated with the presence of nanoscale IL pools containing both onium and Ag ion species at the film surface play a crucial role in the observed antimicrobial activity.

The retention of silver within a composite matrix is an important consideration for utilizing the final material in antimicrobial coating applications. For example, it is necessary to ensure that Ag present within such a coating is sustainably released and is not catastrophically lost upon repeated use. In order to test for this feature, we performed a series of antimicrobial experiments with the same surface and we find that the antimicrobial activity of our films is reproducibly retained for at least five cycles. We believe that the unique macroporous texture of these composites contributes to this sustained antimicrobial activity. In particular, the dispersed nanoscale IL pools within the pitted porosity result in a continuous exposure of bacterial cells to alkylammonium and silver cations to induce rapid bacterial killing at zones near the film surface. The dispersed phase-separated IL provides an abundant reservoir of both onium and silver ions on the surface and the uniform distribution of the IL phase across the entire thickness of the films ensures that these coatings are self-regenerating, even during mechanical wear, an ideal attribute for real world decontamination applications.

CONCLUSIONS

In summary, we introduce here a new approach toward composite antimicrobial films which marries the attractive features of stable OSNP-based sol−gel-derived matrices (i.e., transparency, hydrophobicity, surface tunability) with an apparently well-distributed Ag^+ population arising from inclusion of an IL phase containing a colloidal silver ionosol produced by direct sputtering into the IL. Interestingly, the choice of IL exerts a profound influence over the observed antimicrobial activity, an outcome linked to the porous architecture of the silica and the IL-assisted mechanism of microbial attack by silver. The reasons behind this remarkable behavior form the basis for ongoing studies in our group. At any rate, the synergistic merger of these two technologies yields tailored materials with excellent features and suggests future promise for fabricating long-lived, sustained antimicrobial surfaces and other novel, multifunctional coatings of interest in sensing, drug delivery, and catalysis.

ASSOCIATED CONTENT

Supporting Information

Includes UV−vis absorbance spectra of IL with AgNPs subjected to HCl; XRD of IL with AgNPs and sample 6; and EDS analysis of sample 6. This material is available free of charge via the Internet at http://pubs.acs.org.

AUTHOR INFORMATION

Corresponding Author

*E-mail: gangopadhyays@missouri.edu (S.G); bakergar@missouri.edu (G.A.B); korampallyv@missouri.edu (V.K).

ACKNOWLEDGMENTS

S.G. acknowledges the financial support of the National Science Foundation (IIP-0823108) and the Leonard Wood Institute (400-185). G.A.B. thanks the University of Missouri-Columbia

for providing start-up funds used in support of this research. The authors thank Joseph Mathai for his assistance with the XRD measurements.

REFERENCES

(1) Castellano, J. J.; Shafii, S. M.; Ko, F.; Donate, G.; Wright, T. E.; Mannari, R. J.; Payne, W. G.; Smith, D. J.; Robson, M. C. *Int. Wound J.* **2007**, *4*, 114−122.
(2) Lansdown, A. B. G. In *Biofunctional Textiles and the Skin. Current Problems in Dermatology*; Hipler, U.-C., Elsner, P., Eds.; Karger: Basel, Switzerland, 2006; Vol. 33, p 17−34.
(3) Panyala, N. R.; Pena-Mendex, E. M.; Hovel, J. *J. Appl. Biomed* **2008**, *6*, 117−129.
(4) Oyanedel-Craver, V. A.; Smith, J. A. *Environ. Sci. Technol.* **2007**, *42*, 927−933.
(5) Appendini, P.; Hotchkiss, J. H. *Innovative Food Sci. Emerging Technol.* **2002**, *3*, 113−126.
(6) Silvestre, C.; Duraccio, D.; Cimmino, S. *Prog. Polym. Sci.* **2011**, *36*, 1766−1782.
(7) Wang, J.-X.; Wen, L.-X.; Wang, Z.-H.; Chen, J.-F. *Mater. Chem. Phys.* **2006**, *96*, 90−97.
(8) Tashiro, T. *Macromol. Mater. Eng.* **2001**, *286*, 63−87.
(9) Isquith, A. J.; Abbott, E. A.; Walters, P. A. *Appl. Environ. Microbiol.* **1972**, *24*, 859−863.
(10) Copello, G.; Teves, S.; Degrossi, J.; D'Aquino, M.; Desimone, M.; Diaz, L. *J. Ind. Microbiol. Biotechnol.* **2006**, *33*, 343−348.
(11) Tiller, J. C.; Liao, C.-J.; Lewis, K.; Klibanov, A. M. *Proc. Natl. Acad. Sci. U. S. A.* **2001**, *98*, 5981−5985.
(12) Lv, Y.; Liu, H.; wang, Z.; Hao, L.; Liu, J.; Wang, Y.; Du, G.; Liu, D.; Zhan, J.; Wang, J. *Polym. Adv. Technol.* **2008**, *19*, 1455−1460.
(13) Yoon, K. Y.; Byeon, J. H.; Park, C. W.; Hwang, J. *Environ. Sci. Technol.* **2008**, *42*, 1251−1255.
(14) Kaper, H.; Sallard, S. b.; Djerdj, I.; Antonietti, M.; Smarsly, B. M. *Chem. Mater.* **2010**, *22*, 3502−3510.
(15) Kessler, D.; Roth, P. J.; Theato, P. *Langmuir* **2009**, *25*, 10068−10076.
(16) Mackenzie, J. D.; Bescher, E. P. *Acc. Chem. Res.* **2007**, *40*, 810−818.
(17) Schottner, G. *Chem. Mater.* **2001**, *13*, 3422−3435.
(18) Zha, J.; Roggendorf, H. *Adv. Mater.* **1991**, *3*, 522−522.
(19) Korampally, V.; Mamidi, V. K.; Harris, B.; Gangopadhyay, K.; Baker, G. A.; Gangopadhyay, S. *J. Colloid Interface Sci.* **2011**, *364*, 546−554.
(20) Scheeren, C. W.; Hermes, V.; Bianchi, O.; Hertz, P. F.; Dias, S. L. P.; Dupont, J. *J. Nanosci. Nanotechnol.* **2011**, *11*, 5114−5122.
(21) Gelesky, M. A.; Scheeren, C. W.; Foppa, L.; Pavan, F. A.; Dias, S. L. P.; Dupont, J. *Biomacromolecules* **2009**, *10*, 1888−1893.
(22) Franzoi, A. C.; Vieira, I. C.; Dupont, J.; Scheeren, C. W.; de Oliveira, L. F. *Analyst* **2009**, *134*, 2320−2328.
(23) Kilaru, P.; Baker, G. A.; Scovazzo, P. *J. Chem. Eng. Data* **2007**, *52*, 2306−2314.
(24) Torimoto, T.; Okazaki, K.-i.; Kiyama, T.; Hirahara, K.; Tanaka, N.; Kuwabata, S. *Appl. Phys. Lett.* **2006**, *89*, 243117−1−243117−3.
(25) Vanecht, E.; Binnemans, K.; Seo, J. W.; Stappers, L.; Fransaer. *Phys. Chem. Chem. Phys.* **2011**, *13*, 13565−13571.
(26) Kuwabata, S.; Tsuda, T.; Torimoto, T. *J. Phys. Chem. Lett.* **2010**, *1*, 3177−3188.
(27) Luo, H.; Baker, G. A.; Dai, S. *J. Phys. Chem. B* **2008**, *112*, 10077.
(28) Lu, Y.; Ganguli, R.; Drewien, C. A.; Anderson, M. T.; Brinker, C. J.; Gong, W.; Guo, Y.; Soyez, H.; Dunn, B.; Huang, M. H.; Zink, J. I. *Nature* **1997**, *389*, 364−368.
(29) Korampally, V.; Yun, M.; Rajagopalan, T.; Dasgupta, P. K.; Gangopadhyay, K.; Gangopadhyay, S. *Nanotechnology* **2009**, *20*, 425602.
(30) Chang, Y.; Chen, C.-Y.; Chen, W.-C. *J. Polym. Sci., Part B: Polym. Phys.* **2004**, *42*, 4466−4477.
(31) Mock, J. J.; Barbic, M.; Smith, D. R.; Schultz, D. A.; Schultz, S. *J. Chem. Phys.* **2002**, *116*, 6755−6759.
(32) Li, L.; Zhu, Y.-J. *J. Colloid Interface Sci.* **2006**, *303*, 415−418.
(33) Choi, O.; Deng, K. K.; Kim, N.-J.; Ross, L. Jr; Surampalli, R. Y.; Hu, Z. *Water Res.* **2008**, *42*, 3066−3074.
(34) Mamontov, E.; Baker, G. A.; Luo, H.; Dai, S. *ChemPhysChem* **2011**, *12*, 944−950.
(35) Dizman, B.; Elasri Mohamed, O.; Mathias Lon, J. In *Smart Coatings II*; American Chemical Society: Washington, D.C., 2009; Vol. *1002*, pp 27−51.
(36) Demberelnyamba, D.; Kim, K.-S.; Choi, S.; Park, S.-Y.; Lee, H.; Kim, C.-J.; Yoo, I.-D. *Bioorg. Med. Chem.* **2004**, *12*, 853−857.